Plants, Vital Players in the Terrestrial Water Cycle

van den Berg, Tomas E.; Dutta, Satadal; Kaiser, Elias; Vialet-Chabrand, Silvere; van der Ploeg, Martine; van Emmerik, Tim; Coenders-Gerrits, Miriam; ten Veldhuis, Marie Claire

DOI
10.1007/978-3-031-08262-7_10

Publication date
2022

Document Version
Final published version

Published in
Springer Water

Citation (APA)
van den Berg, T. E., Dutta, S., Kaiser, E., Vialet-Chabrand, S., van der Ploeg, M., van Emmerik, T., Coenders-Gerrits, M., & ten Veldhuis, M. C. (2022). Plants, Vital Players in the Terrestrial Water Cycle. In *Springer Water* (pp. 223-250). (Springer Water). Springer Nature. https://doi.org/10.1007/978-3-031-08262-7_10

Chapter 10
Plants, Vital Players in the Terrestrial Water Cycle

Tomas E. van den Berg, Satadal Dutta, Elias Kaiser, Silvere Vialet-Chabrand, Martine van der Ploeg, Tim van Emmerik, Miriam Coenders-Gerrits, and Marie-Claire ten Veldhuis

Abstract Plant transpiration accounts for about half of all terrestrial evaporation. Plants need water for many vital functions including nutrient uptake, growth and leaf cooling. The regulation of plant water transport by stomata in the leaves leads to the loss of 97% of the water that is taken up via their roots, to the atmosphere. Measuring plant-water dynamics is essential to gain better insight into its roles in the terrestrial water cycle and plant productivity. It can be measured at different levels of integration, from the single cell micro-scale to the ecosystem macro-scale, on time scales from minutes to months. In this contribution, we give an overview of state-of-the-art techniques for plant-water dynamics measurement and highlight several promising innovations for future monitoring. Some of the techniques we will cover include: gas exchange for stomatal conductance and transpiration monitoring, lysimetry, thermometry, heat-based sap flow monitoring, reflectance monitoring including satellite remote sensing, ultrasound spectroscopy, dendrometry, accelometry, scintillometry, stable water isotope analysis and eddy covariance. To fully assess water transport within the soil-plant-atmosphere continuum, a variety of techniques are required to monitor environmental variables in combination with biological responses at different scales. Yet this is not sufficient: to truly account for spatial heterogeneity, a dense network sampling is needed.

T. E. van den Berg
Integrated Devices and Systems, University of Twente, Enschede, The Netherlands

S. Dutta
Dynamics of Micro and Nanosystems, Delft University of Technology, Delft, The Netherlands

E. Kaiser · S. Vialet-Chabrand
Horticulture and Product Physiology, Wageningen University and Research, Wageningen, The Netherlands

M. van der Ploeg · T. van Emmerik
Hydrology and Quantitative Water Management, Wageningen University and Research, Wageningen, The Netherlands

M. Coenders-Gerrits · M.-C. ten Veldhuis (✉)
Water Resources, Delft University of Technology, Delft, The Netherlands
e-mail: J.A.E.tenVeldhuis@tudelft.nl

A. Di Mauro et al. (eds.), *Instrumentation and Measurement Technologies for Water Cycle Management*, Springer Water, https://doi.org/10.1007/978-3-031-08262-7_10

10.1 Introduction

10.1.1 Terrestrial Water Cycle and the Role of Transpiration

Fresh water is a scarce resource in many regions of the world, and around 70% is used by agriculture [1]. It is the most important factor determining crop yields in countries with less industrialized agricultural practices, where the greatest share of agriculture depends on rainfall for its water supply [2]. Global environmental change will likely change the evaporative demand and rainfall in these regions, intensifying the competition between water use for agriculture and human consumption [3]. Plants, and especially irrigated crop plants, require large amounts of fresh water for growth. For example, producing 1 kg of cereal requires 1–3 tonnes of fresh water, putting a high price on food security and water availability [3]. Plants use water in their circulatory system (e.g., to move nutrients), and transpiration of water vapor from the plant to the atmosphere drives exchange from the roots to the rest of the plant. Leaf transpiration provides a cooling mechanism and is a prerequisite for CO_2 uptake and plant growth. Thus, plants have an intimate relationship with water: they need it for their basic functions, growth and reproduction, but 97% of water taken up by plants is lost to the atmosphere as water vapor, accounting for more than 95% of evapotranspiration in certain ecosystems [4]. Future population growth and its increased food demand are likely to exacerbate current scarcities of fresh water [5], as is the increasing salinization of agricultural areas, which itself is caused to a large extent by the soil water flows triggered by transpiration [6]. Therefore, we are in dire need of crops with better water use efficiency and sensors that allow agricultural water users to adjust water supply better to the exact needs of plants.

10.1.2 Water Movement in the Plant

Water and nutrient uptake by the roots, and upwards movement through the plants' vasculature, are driven by a negative hydrostatic pressure in the leaves, which builds up by water lost through transpiration. Water is moved upwards through the plant, if the hydrostatic pressure potential in the leaves is more negative than the combination of matrix potential (e.g., capillary action), soil osmotic potential (i.e., movement of water across a semipermeable membrane) and gravitational potential in the canopy (i.e., force exerted by gravity due to the height of the water column in the plant). Redwoods (*Sequoia sempervirens*), the tallest trees on earth (up to 120 m long) can build up a hydrostatic pressure potential of up to −1.9 MPa in their uppermost leaves, making it possible to move water against gravity to such heights [7]. Long-distance transport of water in the plant is facilitated by the xylem, a specialized vascular system consisting of long, connected cells that function similarly to pipes. Mature xylem vessel cells are dead and empty by design and have a small resistivity to water

movement. The xylem vascular system starts in the root, extends throughout the stem and branches, and delivers water and solutes directly to the leaves, which are the main sites of transpiration.

10.1.3 Root-Soil Water Exchange

The roots are the plant organ for water uptake from the soil and thus the first location where changes in water supply are perceived. The root system consists of a complex architecture of primary and lateral roots which vary in length, number and diameter. Together with cell size and the capillary forces in the plant and soil, they determine root water uptake ability. Coarse roots, the first roots to emerge from the seed, determine the depth of rooting and thereby the uptake of water from deeper soil layers. Root morphological plasticity enables plants to maintain water uptake from deeper layers when drought occurs [8, 9]. In addition, their traits determine the ability to grow in compact soil. The lateral roots that branch from other roots form a dense network of fine roots with root hairs that directly interact with soil particles and extract water and nutrients from them. Water absorption in the roots takes place through active and passive processes. Root cells require energy (ATP) to absorb minerals from the soil; the increased concentration of minerals in the roots generated by this process reduces root water potential relative to its surroundings, thus driving water absorption through endosmosis. Most water absorption through the roots is passive and directly driven by the negative water potential, which is created by the transpiration of water from the air-exposed parts of the plants, mainly through the stomata.

10.1.4 Stomata

Diffusion, the movement of molecules from high to low concentration areas, is the main mechanism of transpiration. Gas diffusion mainly happens through stomata, tiny adjustable pores surrounded by a pair of guard cells and embedded mainly in the leaf surface, but also present in a smaller numbers in other plant organs (e.g., stem). Apart from the stomata, the leaf surface is covered by a waxy layer called the cuticle, which is largely impenetrable to water. Stomata constantly adjust a trade-off between the diffusion of CO_2 into the leaf and the diffusion of water vapor out of the leaf, by opening and closing in response to numerous internal and external cues. For example, high light intensity, low atmospheric CO_2 concentration ($[CO_2]$), and high air humidity all lead to stomatal opening, whereas the opposite situation (low light intensity, high $[CO_2]$, low air humidity) leads to stomatal closure. Further, several stresses, such as drought, soil salinity, heatwaves, ozone and several pathogens trigger stomatal closure, greatly reducing the rate of transpiration as well as photosynthesis and growth. Stomata open when guard cells swell upon active water

uptake (following ion up-take, which increases their osmotic potential), leading to a widening of the stomatal pore. There is a large diversity in the shape of stomata that influences their functionality [10], and their number and pattern across the leaf surface vary depending on plant growth conditions [11]. Up to 900 stomata can cover every mm^2 of leaf surface, and although this is only 0.3–5% of the surface of the leaf, they are responsible for 95% of terrestrial transpiration. The concentration gradient of water vapor inside and outside the leaf is strongly dependent on temperature and air humidity but is generally several orders of magnitude larger than the corresponding [CO_2] gradient. Therefore, to fix 1 mol of CO_2, leaves must transpire approximately 400 mols of water. The current increase in atmospheric [CO_2] may reduce plant transpiration, as elevated [CO_2] leads to a higher water use efficiency of CO_2 uptake, but this effect may be counteracted by a simultaneous increase in leaf and air temperature [12].

10.1.5 Atmosphere and Soil Effects on Transpiration

Even though stomata can control transpiration, different meteorological processes influence the concentration gradient of water between leaf and atmosphere [13]. Changes in net radiation received, air relative humidity, air temperature and wind speed influence transpiration independently of stomatal control. Therefore, the role of stomatal conductance also depends on environmental variables that need to be assessed at different scales [14]. An example is boundary layer conductance, representing a resistance to diffusion at the surface of the leaf that is influenced by leaf geometry and wind speed. Within the canopy, boundary layer conductance (g_b) acts in series with stomatal conductance (g_s) and can represent a substantial limitation of transpiration under certain circumstances (e.g., large leaf, low wind speed). Boundary layer conductance also occurs at the scale of the canopy and limits the rate of water vapor exchange between the canopy and atmosphere. Water availability in the soil, and resistance to water transport within the plant, represent additional factors that can limit transpiration and force stomata to close to maintain the plant's water status. Under drought, if stomatal closure is not sufficient to maintain plant water status, plants can alter their osmotic potential and cell turgor (force of the liquid in a plant cell exerted on its own cell wall), to limit water loss by transpiration. In this case, humidity within the leaf can decrease below the saturation point of water vapor, an essential assumption for most techniques used to measure stomatal conductance.

10.1.6 Measuring Plant Water Relations: Where and How

To fully assess water transport within the soil-plant-atmosphere continuum, a variety of techniques is required to monitor environmental variables and biological responses at different scales (Fig. 10.1). Plant water relations can be monitored at many levels

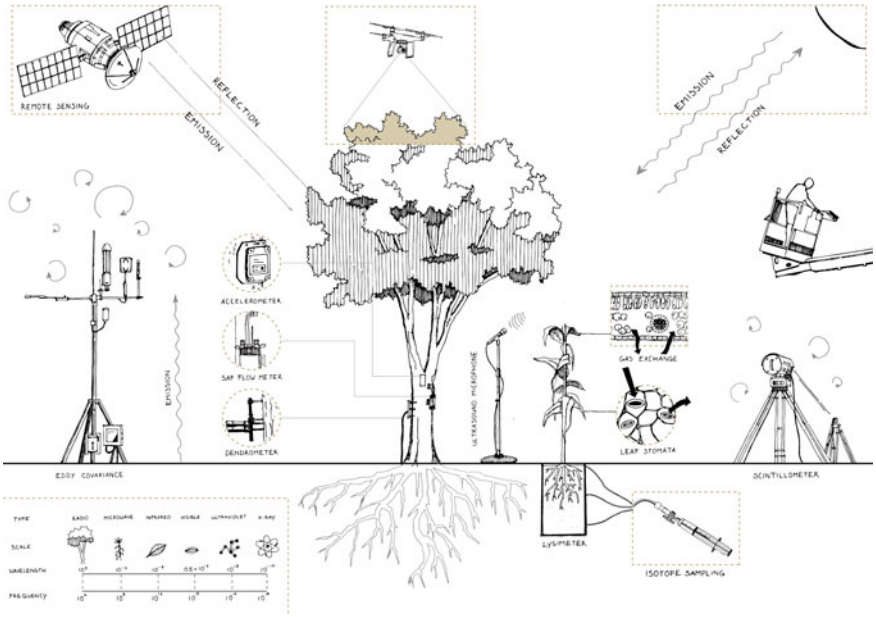

Fig. 10.1 Graphical impression of the different techniques to measure Plant water status and dynamics (by Cher van den Eng)

of integration, from single cells to hectares of canopy, and from minutes to months. In the following sections, we aim to give an overview of the various techniques for monitoring such relations, which are briefly summarized in (Table 10.1).

10.2 Measuring Techniques for Stomatal Conductance and Water-Vapor Exchange at the Leaf Atmosphere Interface

10.2.1 Microscopy

Stomatal conductance to water vapor (g_s), the rate of passage of gasses through the stomatal pore, is defined mainly by the number and pore size of stomata. A diffusion-based equation allows for calculation of g_s from leaf anatomical traits and to estimate the theoretical maximum gas diffusion rate [15–17]:

$$g_s = \frac{\frac{d}{v} Da}{(l + \frac{\pi}{2}\sqrt{(\frac{a}{\pi})}} \tag{10.1}$$

Table 10.1 Overview of available methods and their respective areal scale, temporal scale, measuring principle and sample

Technology	Areal scale	Temporal scale	Measuring principle	Sample
Microscopy	μm^2-cm^2	min	VIS-NIR imaging (nm)	Leaf surface (stomata)
Gas Exchange	cm^2	s-min	IR spectroscopy (μm)	Water vapor
Thermometry	cm^2-km^2	s-min	Thermal IR imaging (μm)	Leaf surface
Scintillometry	m^2-km^2	hour-day	Refractive index NIR spectroscopy (nm-μm)	Air above canopy
Eddy Covariance	km^2	hours	IR spectroscopy (μm) Temperature (T) and velocity (m s^{-1})	Water vapor Air
Dielectric Constant	cm^2	min	Microwave scatter (mm)	Plant tissues
Hyperspectral Imaging	cm^2-km^2	min	Reflectance Imaging (nm-mm)	Plant tissues
Ultrasound spectroscopy	cm^2	s	MegaHz spectroscopy	Plant tissues
Ultrasound xylem cavitations	μm	s	Ultrasound spectroscopy	Air bubble cavitations
Accelerometry	cm^2	s-min	Sway (m s^{-2})	Trees
Field Radar	m^2-km^2	min-hours	Microwave scatter (mm)	Plant tissues
Lysimetry	cm^2	hours	Weighting (g-kg)	Water reservoir
Sap Flow Measurements	cm^2	s	Heat balance	Plant stem
Dendrometry	cm^2	hours	Diameter (mm-m)	Plant stem
Stable water isotopes	cm^2	hours-weeks	Fractionation	Water or water vapor

where d is the diffusivity of water vapor in air (m^2 s^{-1}), v is the molar volume of air (m^2 mol^{-1}), D the stomatal density (nr m^{-2}), a is the stomatal pore area (m^2) and l its depth (m); note that d and v are both temperature and air pressure dependent. $\frac{\pi}{2}\sqrt{\frac{a}{\pi}}$ represents an "end correction", an additional diffusive resistance that is related to converging and diverging concentration shells at both ends of the stomatal pore. Different corrections are possible, depending on stomatal architecture and distribution over the leaf (clustering), which are important to produce accurate g_s estimates [18].

The stomatal pore is often assumed to be elliptical, and the area is estimated from the width and length of the aperture. D is estimated using a microscope by counting the number of stomata per unit area (e.g., field of view) over different areas and each side of the leaf. This takes into consideration the heterogeneous stomatal distribution across the leaf surface. Steady-state stomatal aperture is measured on many stomata acclimated to one condition (combination of temperature, humidity, $[CO_2]$, etc.). In contrast, kinetics of stomatal movement are measured by continuous observation of a limited number of stomata during a change in conditions. Individual, neighboring stomata can show a large variety of responses despite being subjected to the same stimuli, and several stomata need to be measured to represent the overall response at leaf level. Microscopy is useful to obtain a better understanding of plant water relations at the level of single stomata, but currently of limited use for plant monitoring in the field, due to its high cost and labor-intensive employment. However, with more autonomous systems, microscopy could provide solutions for g_s monitoring in uniform and stable environments, such as vertical farms or greenhouses.

10.2.2 Gas Exchange Measurements

Gas exchange is measured by enclosing a part or a complete plant inside a chamber where the environment is controlled. Water vapor concentration can be measured using an infrared gas analyzer (IRGA) or a capacitive humidity sensor. In the case of an IRGA, the concentration of water vapor in an air sample is proportional to the radiation absorbed by water molecules at specific sub-millimeter infrared wavebands, giving a characteristic absorption spectrum [19]. The absorption follows the Beer-Lambert Law and is therefore dependent on the radiation pathway and the concentration of water vapor. A capacitive humidity sensor consists of a hygroscopic dielectric material (i.e., a very poor conductor of electric current that tends to absorb water) placed between a pair of electrodes. Absorption of moisture by the dielectric material results in an increase in sensor capacitance, resulting in an increase in circuit current. At equilibrium conditions, the current is proportional to the amount of moisture present in a hygroscopic material and depends on both ambient temperature and ambient water vapor pressure. There are mainly two types of gas exchange chamber, “closed” and “open”, depending on the air flow renewal within the chamber. In a “closed” system, the plant sample is placed within a chamber where the air is recycled, and air water vapor concentration increases due to transpiration. The slope of the increase in water vapor concentration over time is measured over a short period and used to estimate the transpiration rate. A major limitation of this system is that the plant may respond to the changing relative humidity within the chamber during the measurement, which means that the air needs to be dried or renewed for the following measurement. This problem is solved in an “open" system by using a constantly renewed incoming air flow that is altered by the sample when passing through the chamber. The difference in water vapor concentration before and after the chamber is proportional to the transpiration rate. Such a system generally requires two IRGA

to measure the chamber input and output, and requires regular intercalibration of the IRGA, due to possible drift of the signal over time. Based on transpiration, leaf temperature, and the microclimate within the chamber, g_s can be derived, representing the average response of stomata over the leaf surface. To estimate g_s, one needs to assume that the air within the leaf is saturated with water vapor, which is true for well-watered conditions. The water vapor gradient can therefore be calculated based on leaf temperature and surrounding conditions. A constant mixing of air in the chamber enables a large boundary layer conductance to be maintained, thus allowing derivation of g_s from transpiration. Gas exchange measurements are vital for crop science and plant physiology, because of their direct measurements and good temporal as well as areal resolution for individual plants. Examples of field-based measurements exist [20], but these are not wide-spread for general monitoring.

10.2.3 Scintillometry and Eddy Covariance

Turbulent movements of air above a canopy (in the surface boundary layer), called eddies, transport gases including water vapor, and can be used to detect evaporation over a fixed optical path length (scintillometry) or over a variable area (eddy covariance). Scintillation describes changes in the brightness of an object when viewed through a medium [21]. A well-known and readily observable example for scintillations is a twinkling of the air just above roads on hot summer days. Scintillometers use this optical phenomenon by measuring fluctuations in NIR radiation (e.g., at 0.94 μm) transmitted over a defined path (100 m–4.5 km). These fluctuations within the canopy air boundary layer are used to measure the turbulence structure of the air refractive index (caused especially by fluctuations in temperature and humidity). The derived turbulence structure parameter is used with Monin-Oblukhov similarity theory to estimate sensible heat flux, which, with information on available energy, allows estimation of area-averaged water vapour fluxes (see e.g., [22–24]). While scintillometers are most often used to estimate heat fluxes, they have been found to provide accurate estimations of evaporation at longer time scales (days-months; [21, 25]). Eddy covariance functions as a combination of several measuring techniques of the air above the canopy, combined in a single measuring spot: A sonic anemometer measures direction and velocity of air, an IRGA measures water vapor concentration, and a thermistor measures air temperature. Estimation of net exchange between the canopy and the atmosphere uses the sum of the vertical components of fluxes in the passing eddies at a single sensor position (see [26, 27]). Together, these measurements allow calculation of the fluxes of heat and water vapor exchanged between the canopy and the atmosphere. The measurement footprint of this technique varies depending on the direction and force of the wind. Eddy covariance produces the most reliable results over flat terrain with homogenous vegetation and at steady environmental conditions [28]. Data can be logged at 30–60 min time steps during the day, which is faster than e.g. scintillometry. Several hundred sites around the globe continuously log data, and over 2000 annual datasets have been gathered. Eddy covariance

is most often used to estimate carbon flows (with water vapor concentration as a by-product), and results of evaporation are not published as often. Nevertheless, more than 1500 site-years of evaporation have been published [29], enabling one to draw conclusions on plant-climate interactions.

10.3 Measuring Techniques of Water Status and Transpiration from Leaf to Canopy Scale

10.3.1 Thermometry

Measuring leaf temperature is essential to determine the vapor pressure gradient between leaf and atmosphere but can also be used to measure leaf transpiration. Within the leaf, the transition from liquid to gas at the sites of evaporation results in energy loss and leaf cooling. By calculating the leaf energy balance (the sum of incoming and outgoing energies), it is possible to quantify the energy loss due to transpiration [30] via

$$R_n - C - \lambda E = S, \tag{10.2}$$

with R_n the net radiation (W m^{-2}, C the sensible heat transfer (W m^{-2}), λ the latent heat of evaporation of water (J kg^{-1}), E the evaporative flux (kg $m^{-2}s^{-1}$) and S the net physical storage (W m^{-2}) causing the change in leaf temperature [31]. This requires quantification of all incoming radiation (R_n), which can be difficult to estimate over large areas, especially within the canopy, where leaves can have different heights and orientations. Simultaneous measurement of reference materials with known optical and thermal properties can help reduce the complexity of the energy balance equations, by accounting for part of the effects due to the surrounding environment. Contrary to a gas exchange chamber, the plant is undisturbed, enabling the study of transpiration under natural conditions. Estimating g_s from the rate of water loss requires an estimate of the boundary layer conductance g_b, which mainly depends on wind speed and leaf anatomy, and therefore can vary within the canopy. Methods to estimate g_b rely on energy balance to determine the resistance to heat transfer ($=1/g_b$) between an object and the surrounding environment. For example, a heated aluminum plate can be used to estimate g_b, by monitoring the time required for the plate temperature to reach a new equilibrium with the ambient conditions. A large g_b results in rapid equilibration of plate and air temperature. Temperature can be measured using contact and non-contact methods, which differ in terms of precision and accuracy. Contact measurements using thermocouples, thermistors and resistance temperature detectors (RTD) give relatively accurate and precise point estimates of leaf surface temperature. Heat conduction along the cable, surrounding air conditions on the side of the sensor exposed to the air, and temperature gradients within the leaf, can influence the measurements, as the sensor only touches the leaf surface. Non-contact measurements use infrared radiation (IR) emitted by the leaf in the

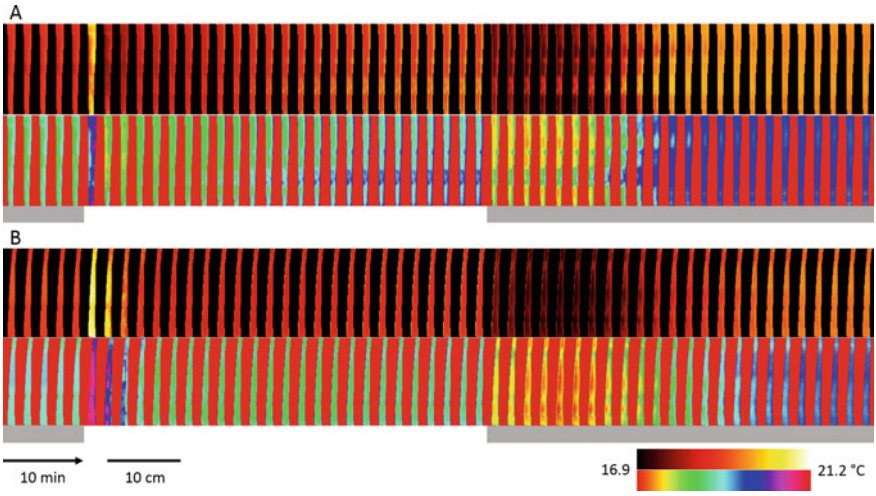

Fig. 10.2 Time series of thermal images displaying leaf temperature spatiotemporal differences for two leaves (A and B) subjected to changes in light intensities (grey background: 0 μmol $m^{-2}\,s^{-1}$, white background: 430 μmol $m^{-2}s^{-1}$). Two different colour scales are used to highlight either temperature kinetics or heterogeneity over the leaf surface. (taken from [31] under CC BY 4.0 License)

0.7–14 μm range to estimate the temperature (T) of any object in the field of view using the Stefan-Boltzmann law

$$\mathrm{IR} = \epsilon\theta T^4, \theta = 5.67 \times 10^{-8}\mathrm{Wm}^{-2}\mathrm{K}^{-4} \tag{10.3}$$

and are generally less precise. Infrared thermocouples and thermal imaging (Fig. 10.1) use this principle and provide estimates that account (to an extent) for the temperature gradient within the leaf. Thermometry using infrared requires knowledge of the emissivity of the object measured (leaf: 0.94–0.96) and is influenced by the infrared radiation emitted by the surrounding objects and their reflection by the sample. The emissivity represents the capacity of the surface of an object to emit energy as infrared radiation and is determined as the ratio (between 0 and 1) of the infrared radiation emitted by the surface of the object and that of the surface of a perfect black body at the same temperature. The higher the emissivity, the stronger will be the signal received from the object by the camera sensor, relatively lowering the effects from the reflected signal due to the surrounding environment. Thermal imaging is a promising technique for transpiration measurements, because it is non-invasive, high-throughput and can cover relatively larger fields of view. Also, as any imaging technique, it provides information on the spatial heterogeneity of the process measured.

Future developments in camera technology and machine vision could enable UAVs to do large scale measurements of not only canopy temperature but also tran-

spiration for more relevant biological interpretation. Satellite thermal imaging uses a coarser methodology compared to thermometry, as reference structures with known optical and thermal parameters are unavailable. Instead, hot and cold pixels are selected; cold pixels represent well-watered plants under non-stress condition with full ground cover, while hot pixels represent bare agricultural land or water-stressed crops with close to zero evaporation [32, 33]. Evaporation is then calculated via the surface energy balance equation, modified as the METRIC Algorithm [34]. The temperature change in the cold pixels is a direct result of stomatal adjustments, which is one of the faster responses to changing water availability. A frequently used measure of water stress is the Crop Water Stress Index (CWSI):

$$CWSI = \frac{T_{\text{canopy}} - T_{\text{wet}}}{T_{\text{dry}} - T_{\text{wet}}} \tag{10.4}$$

With measured canopy temperature T_{canopy}, and upper and lower boundaries for canopy temperature T_{dry} and T_{wet}, respectively. The boundaries correspond to the canopy transpiring equally to the potential evaporation, and the lowest transpiration occurring at high water stress. These can be determined empirically or theoretically. The $CWSI$ is nonlinearly related to canopy transpiration and can change depending on the wind speed conditions (influencing g_b). The actual canopy temperature can be measured from remote sensing imagery, such as from Landsat-8 and Sentinel-2. Examples of applications include water stress monitoring of citrus trees [33]. The main advantage of using thermal methods is that canopy temperature is a faster response to water stress than water potential, vegetation water content, or dielectric properties. However, also thermal reflectance is obstructed by cloud cover, and the revisit time of most available remote sensing missions is not suitable for day-to-day monitoring.

10.3.2 Optical Measurements

The solar radiation that reaches the Earth's surface has its intensity mostly distributed in the wavelength range of 250 nm till 2000 nm. Different bands of the spectrum interact with the leaf and its tissues in different ways. From the viewpoint of a plant's physiology, the spectrum of radiation can be categorized into three functionally relevant groups: (a) ultraviolet UV-B (250–350 nm), (b) Photosynthetically active radiation (PAR) from 380 nm till 750 nm, and (c) near-infrared (NIR) of wavelengths exceeding 750 nm. When light is incident on a leaf surface, it undergoes primarily four kinds of interaction with the cells/tissues. These are (a) Specular reflection, that occurs at the outermost smooth cuticular surface due to a difference in the optical refractive indices at the air-cuticle interface. Specular reflection ($\sim 3\,\%$) is significant at shorter wavelengths of light (250–400 nm) which have a shorter penetration depth; (b) Diffuse reflection [35–38], that occurs at the interfaces of the plant cell walls with the air-spaces deep inside the leaf. This phenomenon is significant for light of wave-

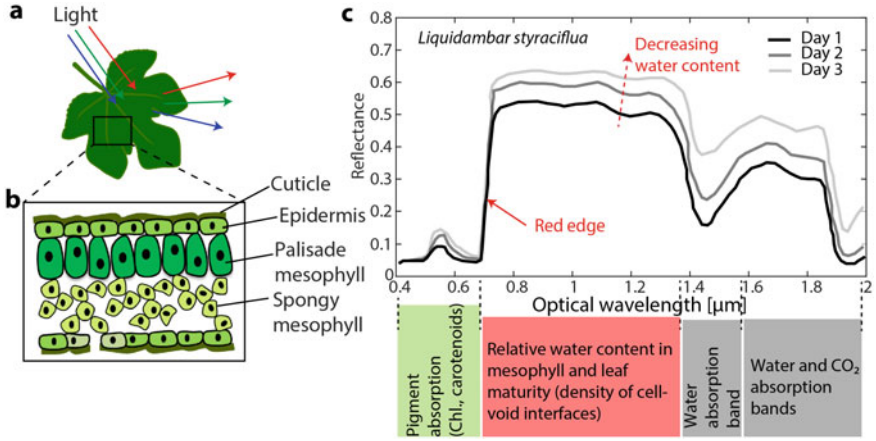

Fig. 10.3 **a** Incident solar radiation undergoes both specular and diffuse reflection from the leaf surface. **b** Schematic cross-section of a typical dicot leaf showing the cuticle, epidermis and the mesophyll tissues. The photosynthetically active radiation gets absorbed mostly in the chloroplasts of the upper palisade cells (having a higher chlorophyll concentration). The NIR components in the light scatters at the cell-air boundaries of the deeper spongy mesophyll leading to diffuse reflection. **c** Spectral reflectance of a single leaf of *Liquidambar styraciflua* [41], measured on indicated days of drought-stress ("Reprinted from Remote sensing of environment, Vol. 30, Hunt Jr, E. R., and Rock, B. N., Detection of changes in leaf water content using Near- and Middle-Infrared reflectances, 43–54, 1989, with permission from Elsevier"). Reflectance increases with decreasing water content. The reflection minima at wavelengths of 420 nm and 650 nm are due to light absorption by chlorophyll. The minima at wavelengths around 1450 nm and 1900 nm are due to absorption by water and carbon dioxide respectively

lengths longer than 400 nm, since the light needs to penetrate to a depth of at least $\sim$ 100 nm before it can interact with different plant cell types; (c) Scattering, that occurs when the size of a particle is similar to the wavelength of the light. Typically, plant cells are larger than 10 μm, and thus do not contribute much to scattering. However, Mie scattering can occur due to the sub-micron sized organelles within the cells [39]; (d) Resonant absorption, that occurs when light of specific wavelengths causes electronic or molecular transitions to excited energy levels. Both photosynthetic pigments, chlorophyll *a*,*b* and carotenoids exhibit absorption bands between 350 and 500 nm, while chlorophyll *a*,*b* has an additional absorption band between 600 and 700 nm [40]. Water molecules exhibit absorption bands in the NIR spectrum e.g., between 1400 and 1500 nm and between 1900 and 2000 nm. The absorbed light energy either is converted to chemical energy during photosynthesis (PAR) or transformed to vibrational energy (heat), leading to a rise in the leaf temperature.

The reflectance spectrum of leaves as shown in Fig. 10.3 is heavily used in remote sensing to monitor the relative water content (RWC). Among the most successful methods to detect water stress are the ones that use reflectance data at two different NIR wavelengths: at 0.76–0.90 μm and at 1.55–1.65 μm) as done by Hunt et al. [41, 42]. The ratio of reflectances $R_{1.6}/R_{0.82}$ is often termed as the Moisture Stress

Index (MSI). The underlying physics behind these techniques is that water absorbs strongly in the band 5 and is quite transparent to band 4, while both wavelengths having a similar reflection coefficient. Another example is the Normalized Difference Infrared Index using the NIR and MIR bands [NDII = (NIR-MIR)/(NIR+MIR)], which correlated highly with canopy water content [43]. Hunt et al. developed an optically derived parameter called as the Leaf Water Content Index (LWCI), defined as:

$$LWCI = \frac{-\log[1-(R_{0.82}-R_{1.6})]}{-\log[1-(R_{0.82}-R_{1.6}^{FT})]} \tag{10.5}$$

where $R_{0.82}$, and $R_{1.6}$ are respectively the reflectance factors measured for the test leaf at 0.82 μm, and 1.6 μm. $R_{1.6}^{FT}$ is the reflectance factor of a reference leaf at full turgor with known RWC. The RWC of a test leaf of weight W can be calculated from the measured dry weight (W^D) and weight at full turgor (W^{FT}) as:

$$\text{RWC} = \frac{(W-W^D)}{(W^{FT}-W^D)} \tag{10.6}$$

Additionally, optical remote sensing can estimate the vegetation greenness or vegetation cover. The reflectance spectrum of leaves exhibits a steep edge in the 680–780 nm wavelength interval, coinciding with the sharp transition in the chlorophyll a absorption window. This band is often termed the "red edge" and the first order derivative of reflectance in the red edge is very sensitive to variations in chlorophyll concentration and decreases are a common symptom of nutrient deficiencies (e.g., water). Rather than analyzing the reflectance of a single band, multispectral data is used to calculate indices. The most frequently used index is the Normalized Difference Vegetation Index (NDVI) [44]. NDVI is related to many relevant vegetation properties, such as leaf area index, biomass, chlorophyll concentration, and vegetation cover, and can be calculated using:

$$\text{NDVI} = \frac{\text{NIR}-\text{Red}}{\text{NIR}+\text{Red}} \tag{10.7}$$

With the reflectance in the near infrared (NIR) and for the red band (Red). NDVI is used to estimate transpiration. Although this is mainly based on empirical relations. For example, through multiplying reference evaporation by NDVI-based crop coefficients. A recent study [45] used NDVI derived from Landsat-7 and Landsat-8 imagery to explore the relation with sap flow and transpiration in a temperate forest. A positive correlation was found between the spatial variability in sap flow and NDVI. It was also shown that NDVI follows the sap flow during the beginning of a new cycle of plant growth, demonstrating the potential for plant monitoring. NDVI can also be used to monitor the impact of droughts on vegetation. For example, NDVI derived from the SPOT-Vegetation mission was used to calculate water stress coefficients for croplands and mixed-vegetation areas [46]. Main drawbacks of optical techniques, such as the NDVI, include signal saturation for surfaces with high

biomass, and blocking by cloud cover. Especially the latter makes optical techniques not always suitable for monitoring vegetation dynamics at shorter time scales.

10.3.3 Microwave Measurements

Plant water status has a direct influence on a its dielectric properties, which are a measure of its interaction with microwaves. Microwaves are sensitive to vegetation, because of scattering and attenuation as the signal travels through the vegetation layer. The degree of scattering and attenuation depends on vegetation properties (dielectric constant, geometry, architecture), and microwave characteristics (frequency, incidence angle, polarization). For example, higher frequencies (shorter wavelengths) are more likely to be directly reflected by the canopy, and lower frequencies (longer wavelengths) penetrate further through the vegetation layer. In remote sensing, microwaves are used in either passive or active methods. Active methods (radar) emit microwaves and measure the reflected backscatter. Passive methods (radiometry) only measure the naturally emitted, and attenuated, microwaves. Initially, understanding the variation in vegetation dielectric properties were mainly interesting for (space-born) radar and radiometer applications. The dielectric constant is an important parameter in several models that relate plant water status to microwave backscatter. However, the emergence of in-vivo dielectric measurement methods also offers the possibility to directly monitor plant water status non-destructively. Examples include the use of a microstrip line resonator, coupled to a vector network analyzer (VNA) (Fig. 10.4). Per measurement, the reflection coefficient of the emitted signal is measured, which depends on the dielectric constant of the sample. So far it has been shown, in corn and tomato leaves, that dielectric responses are directly coupled to leaf gravimetric leaf water content (Fig. 10.5) [47, 48].

Field-based radars can be used to monitor vegetation water status with high spatial and temporal frequency. Both soil moisture and plant water content affect the total backscatter. Higher soil moisture result in higher direct scatter from the soil.

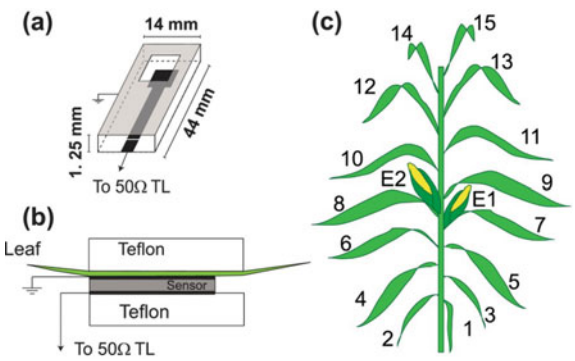

Fig. 10.4 **a** Microstrip line resonator used for in-vivo dielectric measurements. **b** Illustration of leaf sample placement. **c** Schematic of a corn plant including leaf and ear numbering (taken from [48] under CC BY 4.0 License)

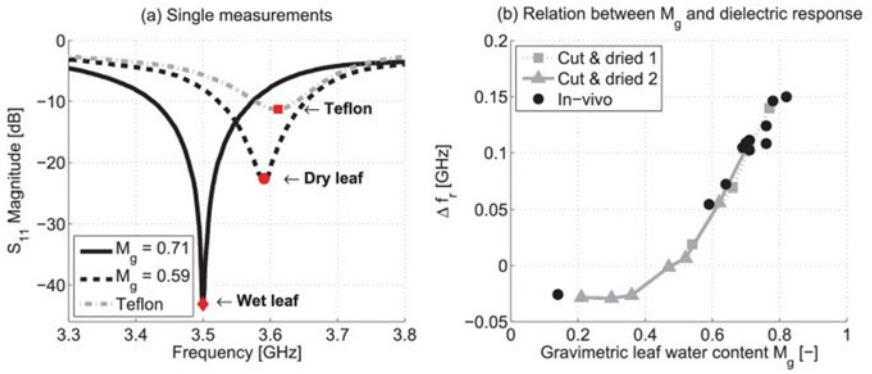

Fig. 10.5 **a** Comparison of dielectric response for dry and wet leaves, and **b** for leaves with varying gravimetric leaf water content (taken from [48] under CC BY 4.0 License)

Increased plant water content increases the direct backscatter from vegetation but can also increase the attenuation of the soil backscatter component. During periods of decreased soil moisture availability, the backscatter is mainly determined by the plant water dynamics. Although to date such setups have mainly been used for fundamental experiments to explore the potential for water status monitoring using remote sensing radar, future developments may result in more cost-effective and practical field-radar systems.

Changes in plant water status in the short (water stress, harvest) or long term (growth, leaf senescence or fall) on large scales are often measured by active and passive microwave methods via satellites. The benefit of using microwave-based methods is the independence of sunlight and cloud cover. For example, RapidScat Ku-band radar aboard the International Space Station was sensitive to vegetation water stress in the Amazon rainforest. Due to its orbit, diurnal cycles of backscatter could be reconstructed monthly. The observed changes in diurnal variability in radar backscatter were associated with changes in water status of the canopy measured on the ground [49]. This demonstrated the potential use of such missions for drought detection and monitoring, using radar remote sensing. Radar remote sensing also offers the possibility to use vegetation dynamics as a measure of root zone water availability [8]. Under water-limited conditions, surface and root zone soil moisture dynamics are decoupled. Yet, Sentinel-1 radar backscatter (C-band) was shown to be dominated by vegetation dynamics of the corn canopy, which was directly related to root zone soil moisture [50]. When using radiometry, the Vegetation Optical Depth (VOD) is a good measure of plant-water dynamics, as VOD is determined by canopy biomass and its water content (VWC). There is a linear relation between VOD and VWC, the latter can in turn be linearly or exponentially related to leaf water potential. The correlation of VOD with leaf water potential has been used to determine the isohydricity of vegetation at global scales. Isohydricity is an important factor that determines the response to vegetation water stress [51, 52].

10.4 Measuring Techniques of Plant Water Dynamics

10.4.1 Transpiration Measurements via Sap Flow Dynamics

Measurements of sap flow in plants provide a direct estimate of transpiration, at the whole plant level or for individual branches [53]. Sap flow measurements provide high time resolution and can be automated which makes them particularly useful for in-field studies [54]. Most techniques are based on the application of heat as a tracer for sap movement [55]. Techniques that directly measure sap flow rate (g h^{-1}) are based on external application of heat to the stem and derive flow rate by solving the stem heat balance. Other techniques apply heat pulses or continuous heating through probes inserted into the stem and derive a stem-average heat flux density (cm^3 cm^{-2} h^{-1}) [56].

Measurement of sap flow rate by the stem heat balance method is non-invasive, a heater is wrapped around the stem and enclosed in a layer of cork or similar material, which in turn is isolated by layers of foam and a weather shield to protect from solar radiation. The method can be applied to both woody and herbaceous stems, for stem diameters as small as 2 mm up to 125 mm. Sap flow is derived from the heat balance of the heated stem segment, by applying pairs of thermocouples that measure heat loss in radial and axial (along the stem, in the direction of the sap flow) direction.

$$P = q_v + q_r + q_f \tag{10.8}$$

where P is the applied heating power (in W), q_v, q_r are the rates of vertical and radial heat loss and q_f heat uptake by the moving sap stream (W). The sap mass flow rate (F_m, kg s^{-1}) is derived from

$$F_m = \frac{2q_f}{c_s(\Delta T_a + \Delta T_b)} \tag{10.9}$$

where c_s is the specific heat capacity of the sap and ΔT_a and ΔT_b are temperature differentials across the heated zone.

The main weakness of this method is that it requires in-situ calibration of the effective thermal conductance of the materials surrounding the heater. This is typically done for periods of zero sap flow, which can be difficult to achieve under field conditions.

Heat pulse methods are based on measurement of the velocity of a heat pulse as it is carried by the sap flow. Temperature is measured upstream and downstream of a heat probe that is inserted into the stem. Several approaches have been developed; an example is the Compensation Heat-Pulse velocity method (CHP, illustrated in Fig. 10.6). Here, the velocity of the heat pulse v_h is derived from

$$v_h = \frac{x_d - x_u}{2t_e} \tag{10.10}$$

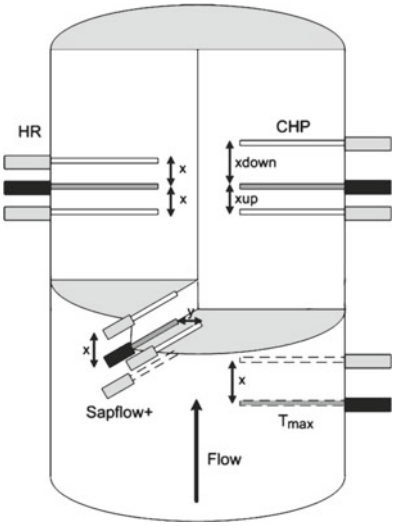

Fig. 10.6 Schematic overview of methods for sap flow measurement based on heat pulse velocity, including CHP, Tmax, Heat ratio and Sapflow+

where x_u and x_d are the distances between the heater and the upstream and downstream temperature sensors and t_e is the time after release of the heat pulse at which the upstream and downstream temperatures are equal. The upstream sensor being closer to the heater than the downstream sensor (Fig. 10.6), t_e equals the time needed for convection in the moving sap stream to move the peak of the heat pulse from the heater to the midway point between the upstream and downstream temperature sensors. The sap flow velocity is derived from the heat pulse velocity by

$$av_s = \frac{\rho_s m c_s m}{\rho_s c_s} \tag{10.11}$$

where a is the fraction of conducting sap wood over the total stem cross-section, ρ and c are density and specific heat capacity of the sap and sap-and-wood-matrix.

Heat pulse methods are based on the assumption that wood is thermally homogeneous, and that equilibration of sap and surrounding wood occurs near-instantaneously. Temperature probes are inserted into the sapwood, at one or more locations downstream and upstream of a heating probe. Several heat pulse methods have been developed apart from CHP, including the Tmax method, Heat Ratio method, calibrated average gradient method and Sapflow+, as illustrated in Fig. 10.6 (see [57] for a complete review). In all heat pulse-based methods, heat pulse velocity is derived from differential temperatures along the axial direction of the stem, in some methods a tangential measurement is added. Heat pulse velocity is converted to flux density by accounting for sapwood water content and sapwood and dry wood density and specific heat capacities. Most heat pulse-based methods, except CHP, require an estimate of sapwood diffusivity which needs to be determined during zero flow conditions or can be determined empirically. Since all sap flux density methods rely on inserting probes into the sapwood, development of wound tissue occurs that locally

alters sapwood properties and heat dissipation. This effect can be limited by regularly relocating the probes. Wound correction equations have been developed for some of the heat-pulse systems. Reliability of the heat-pulse systems is strongly influenced by correct spacing of the temperature probes and by the assumption of thermal homogeneity of the sapwood. Especially for hardwood species non-uniform distribution of sap-conducting tissue this cause deviations in the sap flux density estimates [58].

10.4.2 Dendrometry

Dendrometers can be used to measure the changes in total stem, bark, xylem and phloem width individually. Changes in water content leads to cell shrinking and swelling. In turn the tissue of the stem can vary in size [59]. Dendrometers are placed on the stem or stalk and measure stem diameter variations. Stem variations follow diurnal variations. Depending on the isohydricity of the plant, these diurnal variations are affected by changing water availability. Besides short-term changes in stem width, dendrometers can also be used to monitor longer-term changes in stem radius. These changes can be related to plant growth and can give additional insight in the extent to which optimal crop growth is obtained [59].

10.4.3 Lysimetry

Lysimeters are often used to study the relation between the water cycle and vegetation, for example to quantify seasonal changes. Weighable lysimeters allow for precise quantification of the water balance terms at the soil plant atmosphere interface. Weighable lysimeters are often equipped with soil sensors, to follow processes in the soil which may change over time (e.g. [60]) or have a direct relation with plant physiology [61]. For monitoring soil water processes two often employed techniques are sensors for water content and for the water potential (e.g. [62]). Together these sensors can be used to determine the water retention characteristic of a soil, and the soil hydraulic conductivity. Lysimeters typically range from pot experiments (see above) to 12 m^3 [63]. For determining the water balance at larger scales, radar interferometry has been identified as a potential technique for soils with swelling and shrinking properties [64]. In addition lysimeter results can be spatially extrapolated using thermal imaging [65].

10.4.4 Stable Water Isotopes Measurements

The use of stable water isotopes to study water behavior and flow paths has become more common in the last decades (e.g., [66, 67]). Stable water isotopes are considered

an ideal tracer, as the oxygen (^{18}O and ^{16}O) and hydrogen (^{2}H and H) atoms of water molecules are stable and naturally present in water.

Stable water isotopes are particular of interest to partition total evaporation (E_{tot}) into transpiration (E_t) and soil evaporation (E_s) (e.g., [68–70]). The fact that during evaporation, the light isotopes (^{16}O and H) are preferred to evaporate, results in an enrichment of heavy isotopes (^{18}O and ^{2}H in the remaining residue, e.g., the soil [71]. This process is called fractionation. For root water uptake (transpiration) fractionation does not occur: the plant just takes the available water without changing the isotopic ratio [72]. This distinct difference allow to partition total evaporation.

The isotopic ratio of heavy over light isotopes (R) is often expressed in comparison to the Vienna Standard Mean Ocean Water (VSMOW):

$$\delta_{\text{sample}} = \left(\frac{R_{\text{sample}}}{R_{\text{VSMOW}}} - 1 \right) \times 1000‰ \tag{10.12}$$

By means of a simple isotopic mixing mass balance ($\delta_{E_{\text{tot}}} \cdot E_{\text{tot}} = \delta_{E_t} \cdot E_t + \delta_{E_s} \cdot E_s$), the transpiration ratio can be calculated via the 'isotopic-two-source-model' [73]:

$$\frac{E_t}{E_{\text{tot}}} = \frac{\delta_{E_{\text{tot}}} - \delta_{E_s}}{\delta_{E_t} - \delta_{E_s}} \tag{10.13}$$

The main challenge of this approach is the correct sampling of the isotopic ratios, where minor errors can easily propagate into large uncertainties [74–76]. To estimate $\delta_{E_{\text{tot}}}$ and δ_{E_s}, often the Craig-Gordon model is applied that uses as input water vapor samplings and soil water samplings, respectively [77]. While for δ_{E_t} the water vapor directly originating from the leaves is collected via special chambers [78]. Traditionally, 'cold traps' are used to condensate this water vapor (from the air or leaves) into liquid, so that the sample can be injected into an isotopic ratio mass spectrometer [79, 80]. However, obtaining full condensation without fractionation remains challenging, often leading to erroneous evaporation ratio estimates [81]. Fortunately, recent advances in laser-based instruments allow the direct analysis of water vapor [82–84]. These developments also enabled improved use of the Keeling-plot method [73, 85]. This method assumes that the isotopic concentration in the atmosphere (C_a) is the sum of some background concentration (C_{bg}) plus the concentration from the total evaporation $C_{E_{tot}}$:

$$C_a = C_{bg} + C_{E_{\text{tot}}} \tag{10.14}$$

Combining this via a simple mass balance ($\delta_a C_a = \delta_{bg} C_{bg} + \delta_{E_{\text{tot}}} C_{E_{\text{tot}}}$) the following linear relationship is obtained:

$$\delta_a = C_{bg} \left(\delta_{bg} - \delta_{E_{\text{tot}}} \right) \frac{1}{C_a} + \delta_{E_{\text{tot}}} \tag{10.15}$$

Thus by plotting $1/C_a$ versus δ_a for different heights (or times), the intercept provides the isotopic ratio of the transpiration ($\delta_{E_{\text{tot}}}$). The Keeling plot method works for stable water isotopes as well as for carbon isotopes to estimate e.g., the water use efficiency.

10.5 Novel Approaches to Plant Water Status Measurements

10.5.1 Acoustic Measurements of Leaf and Plant Water Status

10.5.1.1 Multiple Resonant Ultrasound Spectroscopy of Leaves

Unlike light, sound energy does not interfere directly with the physiological activity of plants and can thus be used to monitor the physical state of plant organs non-invasively. Exciting a plant part with acoustic waves at ultrasonic frequencies enables one to probe its inner structure. Leaves, being a few hundred microns thick, are suitable targets for studying their inner structure and water-content via a technique known as non-contact resonant ultrasound spectroscopy (NC-RUS) [86]. When excited with ultrasound (Fig. 10.7a), the transmitted acoustic signal exhibits multiple orders of vibration resonances (Fig. 10.7b) of the leaf and its inner cell structure; the fundamental frequency varies inversely with leaf thickness. The resonant frequency of a vibrating element is a strong function of its elastic modulus (stiffness) and mass density. Both parameters are sensitive to the turgor pressure determined by its water potential. NC-RUS, therefore, provides a way to monitor the in-vivo response of leaf anatomy to drought stress.

A recent study [86, 87] showed how analyzing the higher order acoustic resonances with a metaheuristic two-layered algorithm can lead us to extract the structural and viscoelastic properties of the constituent layers of leaf tissues. These distinguishing traits show up in the extracted acoustic impedances and elastic moduli using NC-RUS and are related to its water status [86].

10.5.1.2 Acoustic Emission from Xylem Vessels

During heavy drought stress, when soil water potential falls below -0.5 MPa, air bubbles may form within xylem vessels as a result of cavitation [89, 90]. Post formation, these bubbles can expand and block the vessels (embolism), thereby hindering water-transport. Vulnerability to cavitation is a popular method to quantify plant drought resistance. Bubble formation in xylem vessels is accompanied by the emission of low intensity sound bursts (see Fig. 10.7c), typically in the far audible and ultrasonic range (frequencies > 10 kHz). Some attempts have been made to understand the underlying characteristics of the emitted sound pulses, although they are

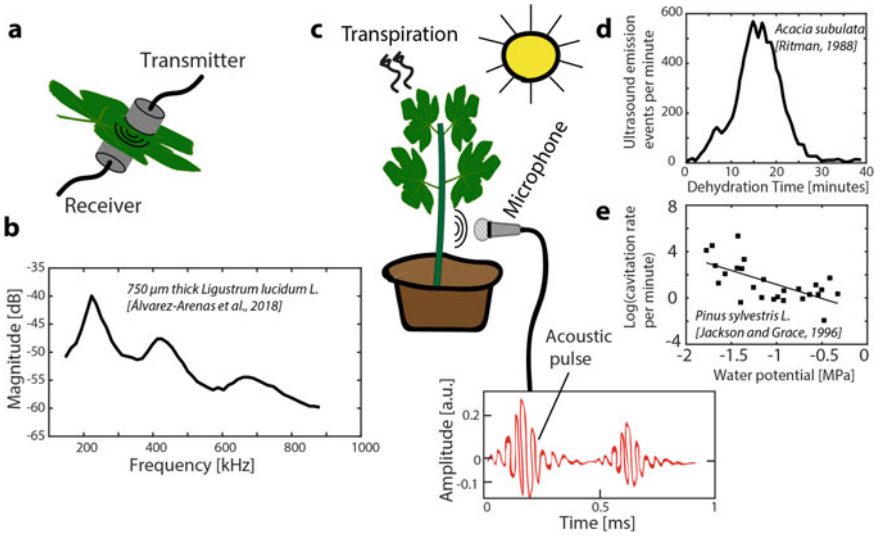

Fig. 10.7 **a** Schematic showing an ultrasound transceiver set-up to perform multiple resonant spectroscopy of a leaf. **b** A typical frequency response of a *Ligustrum lucidum* leaf when ultrasound is transmitted through it [86]. The characteristic peak frequencies represent acoustic resonances in the layered mesophyll tissue of the leaf ("Reprinted from [Álvarez-Arenas, T. E. G., Sancho-Knapik, D., Peguero-Pina, J. J., Gómez-Arroyo, A., & Gil-Pelegrín, E. (2018). Non-contact ultrasonic resonant spectroscopy resolves the elastic properties of layered plant tissues. Applied Physics Letters, 113(25), 253704, with the permission of AIP Publishing"). **c** Plants undergo cavitation in its xylem vessels and emit ultrasound bursts under drought-stress coupled with rapid transpiration. The sound bursts are weak in intensity and resemble damped sinusoidal oscillations containing multiple frequencies; these can be recorded non-invasively with a microphone. **d** A typical evolution of ultrasound emission rate (events per minute) of a drought-stressed *Acacia* tree, as a function of the time of dehydration [88]. **e** The rate of sound emission (events per minute) versus the water potential in *Pinus sylvestris* trees [89]

still at a speculative stage. Ritman and Milburn [88] suggested that the length of the vessels has an influence on the cut-off frequency of the sound: ranging 500 Hz to beyond 100 kHz.

The sum of emission events over time during drought is a good measure of the loss in stem hydraulic conductivity [91–94] and can be used as an indirect and non-destructive marker for drought-stress resistance of a plant. The rate of sound emission events has been observed [89] to roughly follow an exponential dependence on the negative water potential. The emission rate of the sound bursts at first tends to increase with time (as water potential becomes more negative), and eventually decreases and ceases to occur when all vulnerable vessels are embolized [95] (see Fig. 10.7d, e). Further, vessels of larger diameter are more prone to cavitation. In the seminal work by Jackson and Grace [89], a high correlation was observed between acoustic emission rate per minute and the diurnal cycles of PAR and Vapor Pressure Deficit in Scotts Pine trees.

Advances in microelectronics technology have boosted the performance of acoustic sensors. State-of-the-art acquisition systems [96, 97] are able to record and store waveforms from multiple channels at high sampling rates. A popular application of acoustic monitoring is to determine the endpoint of a plant's vulnerability curve (VC), which is a curve of the% loss in hydraulic conductivity versus xylem water potential. The endpoint physiologically corresponds with complete cavitation of the xylem vessels, and thus the full breakdown of the plant's hydraulic pathway. Vergeynst et al. [98] developed a mathematical procedure to determine the endpoint by finding the local maximum of the 3rd derivative of the curve of cumulative acoustic emissions versus time. In another work [99], hydraulic measurements on 16 plant species showed that the highest acoustic activity occurred near the 50 % point of the VC, which is the inflection point.
A plant's response to drought-stress depends on both its physiological and anatomical characteristics [100] and *in vivo* measurements are necessary to map it completely. Conventional methods to determine a plant's vulnerability to cavitation are destructive, and labor-intensive, which hampers their field-applicability. Acoustic (ultrasound) monitoring has the potential to measure non-destructively, enabling automated and continuous measurements in the field.

10.5.2 Accelerometry

Accelerometers can be used to monitor the sway of plants and trees. Sway is determined by physical properties such as biomass and elasticity [101], which in turn are related to water content. Plant mass is directly influenced by the plant water content and the elasticity depends on the stiffness and the density, which are also both affected by water content. Also, plant geometry (size, shape, distribution, orientation of leaves, branches stalks, fruits) influences the sway response to wind forcing [102]. Sway can be used to monitor plant response to water availability, by looking at the change in either their natural frequency or the slope of the power spectrum of sway [103, 104]. Under increased water stress, changes in water content can lead to direct changes in the sway characteristics, offering a direct method to detect and monitor vegetation water stress in the field [105]. Also, accelerometers are relatively inexpensive, allowing for large-scale implementation in-situ.

10.6 Outlook

Plant-based measurement techniques provide direct estimates of leaf and plant water status that are useful to analyze and diagnose behavior of individual plants. For many applications, including those in hydrology, information at higher aggregation levels is required, typically from plot (∼100–1000 m) to ecosystem (∼1–100 km) scale. Depending on the type and scale of the problem at hand, combining in-situ and remote

sensing observations provides a way of bridging the scale gap. However, variability within the grid cell measurement, provided by remote sensing observations, needs to be accounted for. A strategy needs to be adopted that combines in-situ observations at representative locations to cover spatial variability with remote sensing observations that capture spatial average conditions. Especially in areas with complex vegetation and terrain, this can be challenging. Even in managed crop fields, heterogeneities of soil and atmosphere conditions as well natural phenotype variability cause plants to interact differently with their environment. Sparse single measurements nor remote sensing observations can adequately resolve such variability. Solutions are needed that enable ubiquitous in-situ sensing of plant water relations, robustly, autonomously and at limited cost. Current techniques to study plant-water relations strongly rely on measurements at the leaf or plant scale. Upscaling to plant, plot or ecosystem scales requires representative sampling of a sufficient number of specimens to account for vegetation heterogeneity and environmental variability (soil, topography, atmosphere). Remote sensing offers larger-scale observations that help to compare between individual samples and large scale mean behavior, yet they are inevitably indirect observations subject to uncertainties associated with signal conversion. Moreover, satellite or UAV-based remote sensing platforms suffer from low temporal resolution. To truly account for spatial heterogeneity, a dense network sampling is needed. With the advent of low-cost data computing and communication technologies, the only remaining limitation is sensor cost, power, autonomy and robustness. Such multisensory networks with autonomous smart analytics could provide stakeholders with input on transpiration, water content and early stress detection at unprecedented temporal and areal scales. Sensor nodes that combine available (temperature, humidity, wind speed, dendrometry, sap flow) with new sensing methods (RF, hyperspectral, ultrasound, accelerometry) will benefit from more robust data and better stressor identification. Developments in the field of autonomous data acquisition and analysis will largely help to make such sensor networks reality. An example of such a real time, large scale, high frequency and long-term monitoring network is the TREETALKER NETWORK [106], were tree physiological parameters from 600 trees are monitored to determine the impact of climate changes on forests ecosystem services and forest dieback. In addition, the decreasing cost and improvements in the field of thermal and hyperspectral cameras as well as the upgrade of models dealing with such data will boost their use in the monitoring of plant water relations. The use of power generated by the plants rhizosphere itself could even be used to measure autonomously and robustly at remote locations [107]. Together the broad scale of measuring techniques provide an ever-growing choice to fit the stakeholders with the right solution in terms of accuracy, cost, temporal and areal scale to the wide variety of challenges in agriculture and environmental sciences.

References

1. Falkenmark M, Rockstrom J, Rockström J (2004) Balancing water for humans and nature: the new approach in ecohydrology. Earthscan
2. Rosa L, Rulli MC, Davis KF, Chiarelli DD, Passera C, D'Odorico P (2018) Closing the yield gap while ensuring water sustainability. Environ Res Lett 13(10):104002
3. Patrick E (2017) Drought characterization and management in central Asia region and turkey. Technical report
4. Stoy PC, El-Madany TS, Fisher JB, Gentine P, Gerken T, Good SP, Klosterhalfen A, Liu S, Miralles DG, Perez-Priego O et al (2019) Reviews and syntheses: turning the challenges of partitioning ecosystem evaporation and transpiration into opportunities. Biogeosciences 16(19):3747–3775
5. Alexandratos N, Bruinsma J (2012) World agriculture towards 2030/2050: the 2012 revision
6. Rana M, Mark T (2008) Mechanisms of salinity tolerance. Annu Rev Plant Biol 59:651–681
7. Koch GW, Sillett SC, Jennings GM, Davis SD (2004) The limits to tree height. Nature 428(6985):851–854
8. Buitink J, Swank AM, van der Ploeg M, Smith NE, Benninga HJF, van der Bolt F, Carranza CDU, Koren G, van der Velde R, Teuling AJ (2020) Anatomy of the 2018 agricultural drought in the Netherlands using in situ soil moisture and satellite vegetation indices. Hydrol Earth Syst Sci 24(12):6021–6031
9. van der Ploeg MJ, Gooren HPA, Bakker G, de Rooij GH (2008) Matric potential measurements by polymer tensiometers in cropped lysimeters under water-stressed conditions. Vadose Zone J 7(3):1048–1054
10. Tracy L, Jack M (2020) Guard cell metabolism and stomatal function. Ann Rev Plant Biol 71:273–302
11. Hetherington AM, Woodward FI (2003) The role of stomata in sensing and driving environmental change. Nature 424(6951):901–908
12. Ainsworth EA, Long SP (2021) 30 years of free-air carbon dioxide enrichment (face): what have we learned about future crop productivity and its potential for adaptation? Global Change Biol 27(1):27–49
13. Jarvis PG, McNaughton KG (1986) Stomatal control of transpiration scaling up from leaf to region. Adv Ecol Res 15:1–49
14. Jarvis PG (1995) Scaling processes and problems. Plant Cell Environ 18(10):1079–1089
15. Brown HT, Escombe F (1900) Viii. static diffusion of gases and liquids in relation to the assimilation of carbon and translocation in plants. Philos Trans Royal Soc Londn Ser B, Containing Pap Biol Character 193(185–193):223–291
16. Franks PJ, Beerling DJ (2009) Maximum leaf conductance driven by co2 effects on stomatal size and density over geologic time. Proc Natl Acad Sci 106(25):10343–10347
17. Franks PJ, Farquhar GD (2001) The effect of exogenous abscisic acid on stomatal development, stomatal mechanics, and leaf gas exchange in tradescantia virginiana. Plant Physiol 125(2):935–942
18. Peter L, Dani O (2015) Effects of stomata clustering on leaf gas exchange. New Phytologist 207(4):1015–1025
19. Long SP, Farage PK, Garcia RL (1996) Measurement of leaf and canopy photosynthetic co2 exchange in the field. J Experimental Botany 47(11):1629–1642
20. Song Q, Xiao H, Xiao X, Zhu X-G (2016) A new canopy photosynthesis and transpiration measurement system (capts) for canopy gas exchange research. Agric Forest Meteorol 217:101–107
21. Hemakumara HM, Chandrapala L, Moene AF (2003) Evapotranspiration fluxes over mixed vegetation areas measured from large aperture scintillometer. Agric Water Manage 58(2):109–122
22. Meijninger WML, De Bruin HAR (2000) The sensible heat fluxes over irrigated areas in western turkey determined with a large aperture scintillometer. J Hydrol 229(1–2):42–49

23. Thiermann V, Grassl H (1992) The measurement of turbulent surface-layer fluxes by use of bichromatic scintillation. Boundary-Layer Meteorol 58(4):367–389
24. Van Kesteren B, Hartogensis OK, Van Dinther D, Moene AF, De Bruin HAR (2013) Measuring H2O and CO2 fluxes at field scales with scintillometry: part i-introduction and validation of four methods. Agric Forest Meteorol 178:75–87
25. Moorhead JE, Marek GW, Colaizzi PD, Gowda PH, Evett SR, Brauer DK, Marek TH, Porter DO (2017) Evaluation of sensible heat flux and evapotranspiration estimates using a surface layer scintillometer and a large weighing lysimeter. Sensors 17(10):2350
26. Aubinet M, Vesala T, Papale D (2012) Eddy covariance: a practical guide to measurement and data analysis. Springer Science & Business Media
27. Whitehead JD, Twigg M, Famulari D, Nemitz E, Sutton MA, Gallagher MW, Fowler D (2008) Evaluation of laser absorption spectroscopic techniques for eddy covariance flux measurements of ammonia. Environ Sci Technol 42(6):2041–2046
28. Baldocchi DD (2003) Assessing the eddy covariance technique for evaluating carbon dioxide exchange rates of ecosystems: past, present and future. Global Change Biol 9(4):479–492
29. Gilberto P, Carlo T, Eleonora C, Housen C, Danielle C, You-Wei C, Cristina P, Jiquan C, Abdelrahman E, Marty H et al (2020) The fluxnet2015 dataset and the oneflux processing pipeline for eddy covariance data. Sci Data 7(1):1–27
30. Prashar A, Jones HG (2014) Infra-red thermography as a high-throughput tool for field phenotyping. Agronomy 4(3):397–417
31. Silvere V-C, Tracy L (2019) Dynamic leaf energy balance: deriving stomatal conductance from thermal imaging in a dynamic environment. J Experimental Botany 70(10):2839–2855
32. Bastiaanssen WGM, Menenti M, Feddes RA, Holtslag AAM (1998) A remote sensing surface energy balance algorithm for land (sebal). 1. formulation. J Hydrol 212:198–212
33. Sajad J, Shahrokh Z-P, Dev N (2021) Assessing crop water stress index of citrus using in-situ measurements, landsat, and sentinel-2 data. Int J Remote Sensing 42(5):1893–1916
34. Jamshidi S, Zand-Parsa S, Jahromi MN, Niyogi D (2019) Application of a simple landsat-modis fusion model to estimate evapotranspiration over a heterogeneous sparse vegetation region. Remote Sensing 11(7):741
35. Gausman HW, Allen WA, Cardenas R, Richardson AJ (1970) Relation of light reflectance to histological and physical evaluations of cotton leaf maturity. Appl Optics 9(3):545–552
36. Lois G (1987) Diffuse and specular characteristics of leaf reflectance. Remote Sensing Environ 22(2):309–322
37. Knipling EB (1970) Physical and physiological basis for the reflectance of visible and near-infrared radiation from vegetation. Remote Sensing Environ 1(3):155–159
38. Slaton MR, Hunt Jr ER, Smith WK (2001) Estimating near-infrared leaf reflectance from leaf structural characteristics. Am J Botany 88(2):278–284
39. Gates DM, Keegan HJ, Schleter JC, Weidner VR (1965) Spectral properties of plants. Appl Optics 4(1):11–20
40. Croft H, Chen JM (2017) Leaf pigment content. In: Reference module in earth systems and environmental sciences. Elsevier Inc, Oxford, pp 1–22
41. Hunt Jr ER, Rock BN (1989) Detection of changes in leaf water content using near-and middle-infrared reflectances. Remote Sensing Environ 30(1):43–54
42. Hunt Jr ER, Rock BN, Nobel PS (1987) Measurement of leaf relative water content by infrared reflectance. Remote Sensing Environ 22(3):429–435
43. Hardisky MA, Klemas V, Smart M (1983) The influence of soil salinity, growth form, and leaf moisture on the spectral radiance of spartina alterniflora canopies. Photogramm Eng Remote Sensing 49:77–83
44. Yilmaz MT, Hunt Jr ER, Goins LD, Ustin SL, Vanderbilt VC, Jackson TJ (2008) Vegetation water content during smex04 from ground data and landsat 5 thematic mapper imagery. Remote Sensing Environ 112(2):350–362
45. van Dijke AJH, Mallick K, Teuling AJ, Schlerf M, Machwitz M, Hassler SK, Blume T, Herold M (2019) Does the normalized difference vegetation index explain spatial and temporal variability in sap velocity in temperate forest ecosystems? Hydrol Earth Syst Sci 23:2077–2091

46. Abid N, Bargaoui Z, Mannaerts CM (2018) Remote-sensing estimation of the water stress coefficient and comparison with drought evidence. Int J Remote Sensing 39(14):4616–4639
47. van Emmerik T, Steele-Dunne S, Judge J, van de Giesen N (2015) A comparison between leaf dielectric properties of stressed and unstressed tomato plants. In: 2015 IEEE International Geoscience and Remote Sensing Symposium (IGARSS). IEEE, pp 275–278
48. Van Emmerik T, Steele-Dunne SC, Judge J, Van De Giesen N (2016) Dielectric response of corn leaves to water stress. IEEE Geosci Remote Sensing Lett 14(1):8–12
49. van Emmerik T, Steele-Dunne S, Paget A, Oliveira RS, Bittencourt PRL, de Barros FV, van de Giesen N (2017) Water stress detection in the amazon using radar. Geophys Res Lett 44(13):6841–6849
50. Benninga HJF, van der Velde Coleen Carranza R, van Emmerik T, van der Ploeg M. Exploring the sensitivity of vegetation radar backscatter to rootzone soil moisture. Biogeosciences, submitted
51. Frappart F, Wigneron J-P, Li X, Liu X, Al-Yaari A, Fan L, Wang M, Moisy C, Le Masson E, Lafkih ZA et al (2020) Global monitoring of the vegetation dynamics from the vegetation optical depth (vod): a review. Remote Sensing 12(18):2915
52. Konings AG, Gentine P (2017) Global variations in ecosystem-scale isohydricity. Global Change Biol 23(2):891–905
53. Čermák J, Kučera J, Nadezhdina N (2004) Sap flow measurements with some thermodynamic methods, flow integration within trees and scaling up from sample trees to entire forest stands. Trees 18(5):529–546
54. Clearwater MJ, Luo Z, Mazzeo M, Dichio B (2009) An external heat pulse method for measurement of sap flow through fruit pedicels, leaf petioles and other small-diameter stems. Plant Cell Environ 32(12):1652–1663
55. Poyatos R, Granda V, Flo V, Adams MA, Adorján B, Aguadé D, Aidar MPM, Allen S, Alvarado-Barrientos MS, Anderson-Teixeira KJ et al (2021) Global transpiration data from sap flow measurements: the sapfluxnet database. Earth Syst Sci Data 13(6):2607–2649
56. Smith DM, Allen SJ (1996) Measurement of sap flow in plant stems. J Experimental Botany 47(12):1833–1844
57. Vandegehuchte MW, Steppe K et al (2013) Sap-flux density measurement methods: working principles and applicability. Functional Plant Biol 40(3):213–223
58. Víctor F, Jordi M-V, Kathy S, Bernhard S, Rafael P (2019) A synthesis of bias and uncertainty in sap flow methods. Agric Forest Meteorol 271:362–374
59. Zweifel R, Zimmermann L, Newbery DM (2005) Modeling tree water deficit from microclimate: an approach to quantifying drought stress. Tree Physiol 25(2):147–156
60. Robinson DA, Hopmans JW, Filipovic V, van der Ploeg M, Lebron I, Jones SB, Reinsch S, Jarvis N, Tuller M (2019) Global environmental changes impact soil hydraulic functions through biophysical feedbacks. Global Change Biol 25(6):1895–1904
61. van der Ploeg MJ, Teuling AJ (2013) Going back to the roots: the need to link plant functional biology with vadose zone processes. Proc Environ Sci 19:379–383
62. van Der Ploeg MJ, Gooren HPA, Bakker G, Hoogendam CW, Huiskes C, Koopal LK, Kruidhof H, De Rooij GH (2010) Polymer tensiometers with ceramic cones: direct observations of matric pressures in drying soils. Hydrol Earth Syst Sci 14(10):1787–1799
63. Dijkema J, Koonce JE, Shillito RM, Ghezzehei TA, Berli M, Van Der Ploeg MJ, Van Genuchten MTh (2018) Water distribution in an arid zone soil: numerical analysis of data from a large weighing lysimeter. Vadose Zone J 17(1):1–17
64. te Brake B, Hanssen RF, van der Ploeg MJ, de Rooij GH (2013) Satellite-based radar interferometry to estimate large-scale soil water depletion from clay shrinkage: possibilities and limitations. Vadose Zone J 12(3):1–13
65. Voortman BR, Bosveld FC, Bartholomeus RP, Witte JPM (2016) Spatial extrapolation of lysimeter results using thermal infrared imaging. J Hydrol 543:230–241
66. Gat JR (1996) Oxygen and hydrogen isotopes in the hydrologic cycle. Ann Rev Earth Planetary Sci 24(1):225–262
67. Kendall C, McDonnell JJ (2012) Isotope tracers in catchment hydrology. Elsevier

68. Good SP, Soderberg K, Guan K, King EG, Scanlon TD, Caylor KK (2014) δ2h isotopic flux partitioning of evapotranspiration over a grass field following a water pulse and subsequent dry down. Water Resources Res 50(2):1410–1432
69. Jimenez-Rodriguez CD, Coenders-Gerrits M, Wenninger J, Gonzalez-Angarita A, Savenije H. Contribution of understory evaporation in a tropical wet forest. Hydrol Earth Syst Sci 24:2179–2206
70. Youri R, Philippe B, Isabelle B, Laurent C, Jean-Louis D, Jean-Paul G, Patricia R, Michel V, Thierry B (2010) Partitioning evapotranspiration fluxes into soil evaporation and plant transpiration using water stable isotopes under controlled conditions. Hydrol Process 24(22):3177–3194
71. Allison GB, Barnes CJ (1983) Estimation of evaporation from non-vegetated surfaces using natural deuterium. Nature 301(5896):143–145
72. Ehleringer JR, Dawson TE (1992) Water uptake by plants: perspectives from stable isotope composition. Plant Cell Environ 15(9):1073–1082
73. Yakir D, da SL Sternberg L (2000) The use of stable isotopes to study ecosystem gas exchange. Oecologia 123(3):297–311
74. Coenders-Gerrits AMJ, Van der Ent RJ, Bogaard TA, Wang-Erlandsson L, Hrachowitz M, Savenije HHG (2014) Uncertainties in transpiration estimates. Nature 506(7487):E1–E2
75. Phillips DL, Gregg JW (2001) Uncertainty in source partitioning using stable isotopes. Oecologia 127(2):171–179
76. Wei Z, Yoshimura K, Okazaki A, Kim W, Liu Z, Yokoi M (2015) Partitioning of evapotranspiration using high-frequency water vapor isotopic measurement over a rice paddy field. Water Resources Res 51(5):3716–3729
77. Craig H, Gordon LI (1965) Deuterium and oxygen 18 variations in the ocean and marine atmosphere (consiglio nationale delle ricerche laboratorio di geologia nucleare, Pisa, Italy)
78. Wang L, Good SP, Caylor KK, Cernusak LA (2012) Direct quantification of leaf transpiration isotopic composition. Agric Forest Meteorol 154:127–135
79. Sheppard PA (1958) Transfer across the earth's surface and through the air above. Quarterly J Royal Meteorol Soc 84(361):205–224
80. Wen X, Yang B, Sun X, Lee X (2016) Evapotranspiration partitioning through in-situ oxygen isotope measurements in an oasis cropland. Agric Forest Meteorol 230:89–96
81. Griffis TJ (2013) Tracing the flow of carbon dioxide and water vapor between the biosphere and atmosphere: a review of optical isotope techniques and their application. Agric Forest Meteorol 174:85–109
82. Marcel G, Matthias B, Paul K, Heike W, Josefina H, Thomas H (2016) In situ unsaturated zone water stable isotope (2 h and 18 o) measurements in semi-arid environments: a soil water balance. Hydrol Earth Syst Sci 20(2):715–731
83. Rodriguez CDJ (2020) Evaporation partitioning of forest stands: the role of forest structure
84. Patrizia N, Alexander G (2018) High-resolution vertical profile measurements for carbon dioxide and water vapour concentrations within and above crop canopies. Boundary-Layer Meteorol 166(3):449–473
85. Keeling CD (1958) The concentration and isotopic abundances of atmospheric carbon dioxide in rural areas. Geochimica et cosmochimica acta 13(4):322–334
86. Álvarez-Arenas TEG, Sancho-Knapik D, Peguero-Pina JJ, Gómez-Arroyo A, Gil-Pelegrín E (2018) Non-contact ultrasonic resonant spectroscopy resolves the elastic properties of layered plant tissues. Appl Phys Lett 113(25):253704
87. Fariñas MD, Jimenez-Carretero D, Sancho-Knapik D, Peguero-Pina JJ, Gil-Pelegrín E, Álvarez-Arenas TG (2019) Instantaneous and non-destructive relative water content estimation from deep learning applied to resonant ultrasonic spectra of plant leaves. Plant Methods 15(1):1–10
88. Ritman KT, Milburn JA (1988) Acoustic emissions from plants: ultrasonic and audible compared. J Experimental Botany 39(9):1237–1248
89. Jackson GE, Grace J (1996) Field measurements of xylem cavitation: are acoustic emissions useful? J Experimental Botany 47(11):1643–1650

90. Zimmermann U, Haase A, Langbein D, Meinzer F (1993) Mechanisms of long-distance water transport in plants: a re-examination of some paradigms in the light of new evidence. Philos Trans Royal Soc Londn Ser B: Biol Sci 341(1295):19–31
91. Hervé C, Eric B, Stéphane H, Sylvain D, Brendan C, Steven J (2013) Methods for measuring plant vulnerability to cavitation: a critical review. J Experimental Botany 64(15):4779–4791
92. Lo Gullo MA, Salleo S (1993) Different vulnerabilities of quercus ilex l. to freeze-and summer drought-induced xylem embolism: an ecological interpretation. Plant Cell Environ 16(5):511–519
93. Sabine R (2015) A new type of vulnerability curve: is there truth in vine? Tree Physiol 35(4):410–414
94. Vergeynst LL, Dierick M, Bogaerts JAN, Cnudde V, Steppe K (2015) Cavitation: a blessing in disguise? New method to establish vulnerability curves and assess hydraulic capacitance of woody tissues. Tree Physiol 35(4):400–409
95. De Roo L, Vergeynst LL, De Baerdemaeker NJF, Steppe K (2016) Acoustic emissions to measure drought-induced cavitation in plants. Appl Sci 6(3):71
96. Gernot M, Denis C, Dani O (2012) Sources and characteristics of acoustic emissions from mechanically stressed geologic granular media-a review. Earth-Sci Rev 112(3–4):97–114
97. Wolkerstorfer SV, Rosner S, Hietz P (2012) An improved method and data analysis for ultrasound acoustic emissions and xylem vulnerability in conifer wood. Physiologia Plantarum 146(2):184–191
98. Vergeynst LL, Sause MGR, De Baerdemaeker NJF, De Roo L, Steppe K (2016) Clustering reveals cavitation-related acoustic emission signals from dehydrating branches. Tree Physiol 36(6):786–796
99. Markus N, Barbara B, Sabine R, Anton N, Stefan M (2015) Xylem cavitation resistance can be estimated based on time-dependent rate of acoustic emissions. New Phytologist 208(2):625–632
100. McDowell N, Pockman WT, Allen CD, Breshears DD, Cobb N, Kolb T, Plaut J, Sperry J, West A, Williams DG et al (2008) Mechanisms of plant survival and mortality during drought: why do some plants survive while others succumb to drought? New Phytologist 178(4):719–739
101. Van Emmerik T, Steele-Dunne S, Hut R, Gentine P, Guerin M, Oliveira RS, Wagner J, Selker J, Van de Giesen N (2017) Measuring tree properties and responses using low-cost accelerometers. Sensors 17(5):1098
102. Jackson T, Shenkin A, Moore J, Bunce A, Van Emmerik T, Kane B, Burcham D, James K, Selker J, Calders K et al (2019) An architectural understanding of natural sway frequencies in trees. J Royal Soc Interface 16(155):20190116
103. Sethi S, Dellwik E, Angelou N, Bunce A, van Emmerik T, Duperat M, Ruel J-C, Wellpott A, Van Bloem S, Achim A, Kane B, Ciruzzi DM, Loheide II SP, James K, Burcham D, Moore J, Schindler D, Kolbe S, Wiegmann K, Rudnicki M, Lieffers VJ, Selker J, Gougherty AV, Newson T, Koeser A, Miesbauer J, Samelson R, Wagner J, Coomes D, Jackson TD, Gardiner B (2020) The motion of trees in the wind: a data synthesis. Biogeosciences Discuss
104. van Emmerik T, Steele-Dunne S, Gentine P, Oliveira RS, Bittencourt P, Barros F, van de Giesen N (2018) Ideas and perspectives: tree–atmosphere interaction responds to water-related stem variations. Biogeosciences 15(21):6439
105. Ciruzzi DM, Loheide SP (2019) Monitoring tree sway as an indicator of water stress. Geophys Res Lett 46(21):12021–12029
106. Castaldi S, Antonucci S, Asgharina S, Battipaglia G, Marchesini LB, Cavagna M, Chini I, Cocozza C, Gianelle D, La Mantia T et al (2020) The Italian treetalker network (itt-net): continuous large scale monitoring of tree functional traits and vulnerabilities to climate change. In: EGU general assembly conference abstracts, p 20591
107. Sudirjo E (2020) Plant microbial fuel cell in paddy field: a power source for rural area. PhD thesis, Wageningen University